frontiers | Frontiers in Earth Science

TYPE Original Research
PUBLISHED 01 September 2022
DOI 10.3389/feart.2022.994876

OPEN ACCESS

EDITED BY
Shangfeng Chen,
Institute of Atmospheric Physics (CAS), China

REVIEWED BY
Chujie Gao,
Hohai University, China
Yongli He,
Lanzhou University, China
Yaocun Zhang,
Nanjing University, China

*CORRESPONDENCE
Yuan Sun,
sunyuan1214@126.com

SPECIALTY SECTION
This article was submitted to Atmospheric Science, a section of the journal Frontiers in Earth Science

RECEIVED 15 July 2022
ACCEPTED 08 August 2022
PUBLISHED 01 September 2022

CITATION
Lv S, Sun Y, Zhong Z and Shen Y (2022), Possible reasons for the migration of tropical cyclone track over the western north pacific: Interdecadal pacific oscillation modulation.
Front. Earth Sci. 10:994876.
doi: 10.3389/feart.2022.994876

Possible reasons for the migration of tropical cyclone track over the western north pacific: Interdecadal pacific oscillation modulation

Shuo Lv[1], Yuan Sun[1]*, Zhong Zhong[1] and Yixuan Shen[2]

[1]College of Meteorology and Oceanography, National University of Defense Technology, Changsha, Hunan, China, [2]PLA Troop 32033, Haikou, Hainan, China

Recent studies have proposed a relatively reliable metric, i.e., the annual-mean latitude of tropical cyclone (TC) lifetime maximum intensity, to evaluate the observed trend of poleward migration of TC. The documented trend in the existing records of the metric suggests that anthropogenic factors might make considerable contributions to the poleward migration of TC. However, here we show that there is no significant TC migration trend in the western North Pacific (WNP). Instead, large interdecadal variation is found in the WNP TC track over the past 35 years. Rather than the anthropogenic factors, it is the natural variability, especially the Interdecadal Pacific Oscillation (IPO), that plays a key role in modulating the migration of WNP TC track. The IPO-related TC migration is assumed to cause systematic changes (i.e., increases and decreases) in regional hazard exposure and risk. The impact of IPO on the WNP TC migration is attributed to its influences on the large-scale circulation, TC genesis potential index, and the potential intensity in the TC prevailing region of the WNP.

KEYWORDS

tropical cyclones, poleward migration, anthropogenic, natural variability, IPO

1 Introduction

In the context of global warming and considering the economic damages and catastrophes resulting from tropical cyclones (TCs) in various ocean basins, it is of great interest and societal importance to understand whether some changes of the TC activity may occur outside of natural variability and thus can be attributed to anthropogenic forcing (Knutson et al., 2010; Wang et al., 2011; Lee et al., 2012; Kossin et al., 2014; Kossin et al., 2016; Lee et al., 2020). While great progress has been made in evaluating the impact of global warming on TC intensity and TC-induced rainfall (Knutson et al., 2010), by far relatively little is known about the anthropogenically forced changes in the current climate (Wang et al., 2011; Kossin et al., 2014).

Over the past 30 years, the annual-mean latitude where tropical cyclones (TCs) reach their lifetime maximum intensity (LMI) has significantly migrated poleward in the northern and southern hemispheres, which potentially would have profound impacts on life and property safety (Kossin et al., 2014). Increasing mortality risks and hazard exposures from TCs (Peduzzi et al., 2012) may be compounded in coastal cities at higher latitudes, while they might possibly be offset at lower latitudes (Cardon et al., 2012; Kossin et al., 2016). TCs from the western North Pacific (WNP), which is also the most active basin hosting the largest TC genesis numbers on earth, make the largest contribution to the trend of TC poleward migration in the northern hemisphere (Kossin et al., 2014; Kossin et al., 2016).

Recent studies suggested that the observed trend of WNP TC poleward migration can be attributed to a conflation of anthropogenic and natural factors (Shen et al., 2018). With a substantial portion occurring outside the dominant known modes of variability in the region [i.e., El Niño–Southern Oscillation (ENSO) and Pacific Decadal Oscillation (PDO)] (Ho et al., 2004; Camargo et al., 2007a; Liu & Chan, 2008; Kossin et al., 2010; Zhang et al., 2012; Liu & Chan, 2013; Wang & Wang, 2013; Mei et al., 2015), it is argued that the TC migration may be related to other forms of slow decadal forcing (possibly anthropogenic forcing) (Kossin et al., 2014; Kossin et al., 2016). ENSO and PDO are known to affect the large-scale environment and thus the genesis and trajectories of the WNP TCs, which eventually contribute to the WNP TC migration (Kossin et al., 2016; Camargo et al., 2007a). However, other variabilities (except for ENSO and PDO) may also contribute to the WNP TC migration, which, if anything, will raise the uncertainty in the contribution of anthropogenic forcing. The Interdecadal Pacific Oscillation (IPO), which is similar to the PDO but occurs over a wider area of the Pacific (Power et al., 1999; Folland et al., 2002; Henley et al., 2015), is expected to considerably contribute to the WNP TC migration. Nevertheless, no studies on the contribution of IPO to the WNP TC migration have been conducted yet. Moreover, despite some studies on recent changes of TC track and exposure under global warming conditions (Knutson et al., 2010; Wang et al., 2011; Lee et al., 2012; Kossin et al., 2014; Kossin et al., 2016), how the natural variability and anthropogenic forcing affect the WNP TC migration still remain unclear.

Here we try to address these issues by analyzing the observations during the 41-year period of 1980–2020, when the best-track data are considered to be most complete and with the highest quality in terms of both TC position and TC intensity due to the monitoring of geostationary satellites (Kalnay et al., 1996; Knapp & Kruk, 2010; Dee et al., 2011; Kossin et al., 2014). We focus on the contribution of IPO to the observed TC migration in the WNP, which has been proved to be an important issue but is underestimated and even ignored in the previous studies.

2 Data and methods

2.1 Climate index

The index "Niño 3.4" (5°N–5°S, 140°E–145°W) defined over this region is widely used to represent the ENSO index, which is available at http://www.esrl.noaa.gov/psd/gcos_wgsp/Timeseries/Nino34/. The "Pacific Decadal Oscillation" (PDO) is a long-lived El Niño-like pattern of Pacific climate variability (Mantua et al., 1997; Christensen, 2013). The PDO index is defined as the projections of monthly mean SST anomalies onto their first EOF vectors in the North Pacific (north of 20oN) (Mantua et al., 1997). The EOF vectors are derived for the period from 1900 to 1993, and climatological value is defined as monthly mean for the same period. Globally averaged monthly mean SST anomaly is subtracted from monthly mean SST anomaly of the Pacific Ocean north of 20°N before calculation of the first EOF vector for the purpose to remove the effect of global warming. The PDO index is available at https://www.esrl.noaa.gov/psd/gcos_wgsp/Timeseries/PDO/. The Interdecadal Pacific Oscillation (IPO) and the PDO are closely related modes of decadal to interdecadal climate variability in the Pacific Ocean (Mantua et al., 1997; Power et al., 1999; Folland et al., 2002; Christensen, 2013; Henley et al., 2015). The PDO can be considered as the North Pacific node of the Pacific-wide IPO (Power et al., 1999; Folland et al., 2002). The IPO is associated with a distinct "tripole" pattern of SST anomalies, and the IPO Tripole Index (TPI) is calculated as follows based on monthly global SST data (Henley et al., 2015): Firstly, subtract the monthly climatological value from SST in each grid cell to eliminate the seasonal cycle and calculate monthly mean SST anomalies ($SSTA_i$) in the three TPI regions using a chosen base period (1971–2000 used here). TPI regions are defined as follows: region 1 (25°N–45°N, 140°E–145°W); region 2 (10°S–10°N, 170°E–90°W); region 3 (50°S–15°S, 150°E–160°W). Secondly, the TPI is calculated as follows:

$$TPI = SSTA_2 - \frac{SSTA_1 + SSTA_3}{2}$$

The TPI is also available at https://www.esrl.noaa.gov/psd/data/timeseries/IPOTPI/.

SST data are taken from the US National Oceanic and Atmospheric Administration Extended Reconstruction of SST (NOAA-ERSST; Smith & Reynolds, 2003), which is a global gridded dataset reconstructed based on historical observations of SST data using statistical methods. This dataset has spatial

resolution of 2°×2° and temporal resolution of monthly, and the scope of this paper is global (0°–360°, 90°N-90°S).

2.2 Genesis potential index , potential intensity , and large-scale environmental flow

GPI has important indicative significance for the generation of TCs and has been widely used in the study of TCs. Its definition is as follows:

$$\mathrm{GPI} = \left|10^5 \eta_{850}\right|^{3/2} \times (1 + 0.1 \times V_{shear})^{-2} \times \left(H_{600}/50\right)^3 \times \left(PI/70\right)^3$$

Where η_{850} represents the vorticity of 850 h Pa, V_{shear} represents the vertical wind shear between 850 h Pa and 200 h Pa, H_{600} represents the relative humidity of 600 h Pa, and PI is the potential intensity. PI describes the thermodynamically-based maximum TC intensity that the environment will support and thus is closely associated with TC genesis and intensification. In conjunction with the work of Emanuel (1999), it is defined as follows:

$$PI^2 = \frac{C_k}{C_D} \times \frac{T_s}{T_0} \times \left(CAPE^* - CAPE^b\right)$$

where C_k and C_D represent exchange coefficient for enthalpy and drag coefficient respectively, T_s and T_0 represent sea surface temperature and average outflow temperature respectively. CAPE is the convective available potential energy, and $CAPE^*$ represents the CAPE value when an air mass within the radius of the maximum wind speed reaches saturation for the first time under the current SST and barometric conditions. $CAPE^b$ represents the value of CAPE of the air parcel in the surrounding boundary layer atmosphere reduced along the isotherm to the radius of the maximum wind speed. In our study, large-scale environmental flow is mainly represented by 500 hPa geopotential height and 850–300 hPa vertical-mean wind.

Note that the GPI, PI and large-scale environmental flow are all calculated from the National Centers for Environmental Prediction–National Center for Atmospheric Research Global Reanalysis (NCEP–NCAR) (Kalnay et al., 1996) data. This reanalysis dataset is using a state-of-the-art system to perform data assimilation with spatial resolution of 2.5×2.5 and temporal resolution of monthly. In this paper, these data are selected from 1980 to 2015, and the spatial range is the Western North Pacific region (100°E-180°, 0°-60°N).

2.3 TC data

Best-track data are obtained from the International Best Track Archive for Climate Stewardship (IBTrACS) v04r00 (Knapp et al., 2010; Knapp et al., 2018), which is available at http://www.ncdc.noaa.gov/ibtracs/. There are four best-track data provided by four different agencies in the WNP: the Joint Typhoon Warming Center (JTWC), Japan Meteorological Agency (JMA), China Meteorological Administration (CMA), and Hong Kong Observatory (HKO). Note that only TCs with LMI ≥35 kt and ≤1,000 hPa are used in our analysis.

2.4 CMIP5 data

To further examine the impact of anthropogenic forcing on meridional migration of WNP TCs in future, we use an ensemble of TCs generated by 14 CMIP5 models, which includes the twenty-first-century RCP4.5 and RCP8.5 projection simulations (Camargo, 2013). RCP4.5 (RCP8.5) is a scenario that stabilizes radiative forcing at 4.5 (8.5) W m^{-2} at the end of the century. CMIP5 models used in this paper include CanESM2, CCSM4, CSIRO Mk3.6.0, Fgoals-G2, GFDL CM3, GFDL-ESM2M, HADGEM2-ES, and INM-CM4.0. Ipsl-cm5a-lr, MIROC-ESM, MIROC5, MPI-ESM-LR, MRI-CGCM3, and NORESM1-M. RCP4.5 is a stabilization scenario and assumes that climate policies are invoked to achieve the goal of limiting emissions, while RCP8.5 corresponds to the pathway with the highest greenhouse gas emissions and is based on a presumption of no to little change from the present trajectories of greenhouse gas concentrations. RCP4.5 and RCP8.5 scenarios have better model coverage compared to the other scenarios, which is available at https://esgf-node.llnl.gov/search/cmip5/.

2.5 Residual analysis

The significance of residual analysis is to check whether the trend of TC poleward movement is still significant after removing the trend of natural variability from the trend of TC poleward migration. ENSO (PDO, IPO) variability is excluded from the annual-mean TC latitude at the time of LMI (φ_{LMI}) time series by regressing each individual φ_{LMI} series from the various best-track data onto the index of the Niño-3.4 (PDO, TPI) and analyzing the residuals named $\varepsilon_{\text{Niño-3.4}}$ ($\varepsilon_{\mathrm{PDO}}$, $\varepsilon_{\mathrm{TPI}}$). ENSO, PDO, and IPO variabilities are removed from the φ_{LMI} series by regressing the φ_{LMI} series onto the indices of Niño-3.4, PDO and TPI, and analyzing the residuals ($\varepsilon_{\mathrm{ALL3}}$).

3 Result

3.1 Insignificant trends of WNP TC poleward migration

The measurement of φ_{LMI} is much less uncertain, since the absolute LMI can be easily determined based on when the TC has reached its maximum intensity during its lifetime (Kossin et al., 2014). Because of the relatively short period of observation after

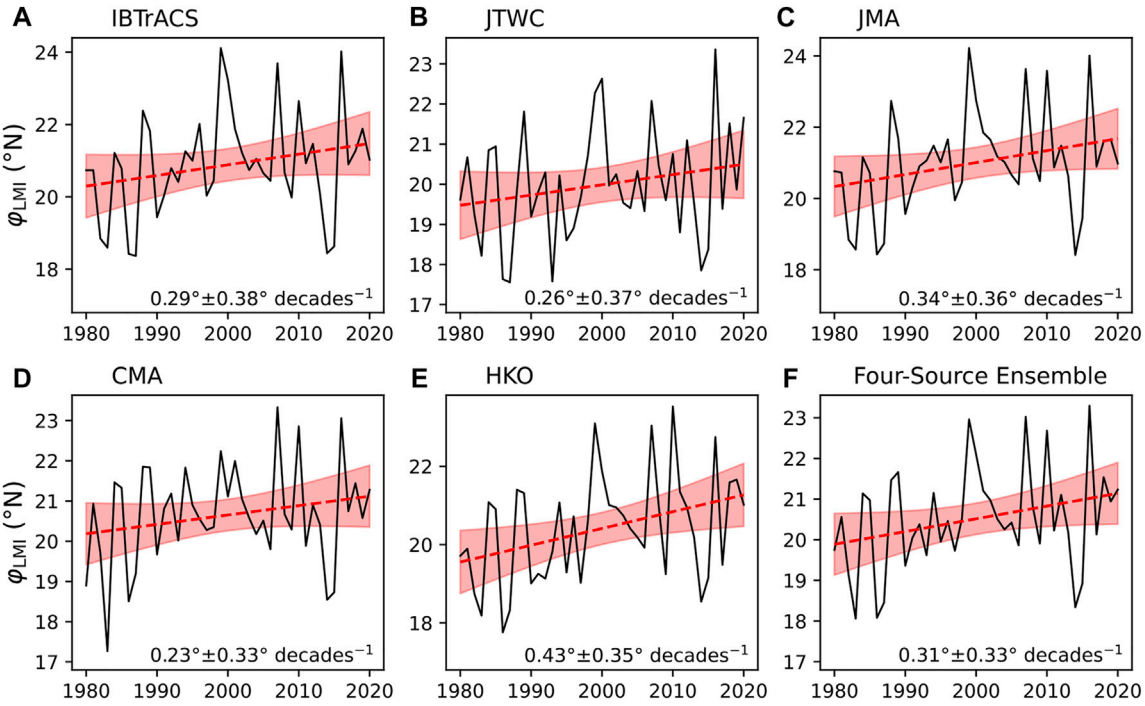

FIGURE 1
Migration of the location of LMI. Time series of annual-mean φ_{LMI} calculated from various best-track historical data over the WNP. **(A–F)** shows data from different sources, where **(A)** is IBTrACS, **(B)** is JTWC, **(C)** is JMA, **(D)** is CMA, **(E)** is HKO and **(F)** is the ensemble mean of JTWC, JMA, CMA and HKO. Linear trend lines (dashed) are shown with their 95% two-sided confidence intervals (shaded), which are also given by the annotated values.

TABLE 1 Linear trends of annual-mean latitude of LMI and its regression residuals for best-track data from various sources. The WNP TC track migration rates and 95% confidence intervals (latitude decade^{-1}) of annual-mean φ_{LMI}, the residuals of the regression of φ_{LMI} onto the JASON-mean Niño-3.4, PDO, and TPI indices (i.e., $\varepsilon_{Niño\text{-}3.4}$, ε_{PDO}, and ε_{TPI}) respectively and the residuals of the trivariate regression of φ_{LMI} onto the three indices (i.e., ε_{ALL3}) for the various best-track data sources. For the single-variate and trivariate regressions, the variance explained R^2 and the p value are also shown.

	IBTrACS	JTWC	JMA	CMA	HKO	Ensemble
φ_{LMI}	0.29 ± 0.38	0.26 ± 0.37	0.34 ± 0.36	0.23 ± 0.33	0.43 ± 0.35	0.31 ± 0.33
$\varepsilon_{Niño\text{-}3.4}$	0.30 ± 0.30	0.26 ± 0.33	0.34 ± 0.29	0.24 ± 0.29	0.44 ± 0.27	0.32 ± 0.27
R^2, p value	0.35, <0.001	0.19, 0.001–0.01	0.31, <0.001	0.21, 0.001–0.01	0.32, <0.001	0.29, <0.001
ε_{PDO}	0.11 ± 0.34	0.08 ± 0.33	0.15 ± 0.33	0.08 ± 0.30	0.21 ± 0.29	0.13 ± 0.28
R^2, p value	0.24, 0.001–0.01	0.22, 0.001–0.01	0.23, 0.001–0.01	0.20, 0.001–0.01	0.26, <0.001	0.29, <0.001
ε_{TPI}	0.03 ± 0.29	0.04 ± 0.31	0.08 ± 0.29	0.04 ± 0.28	0.15 ± 0.25	0.08 ± 0.25
R^2, p value	0.45, <0.001	0.30, <0.001	0.43, <0.001	0.32, <0.001	0.53, <0.001	0.45, <0.001
ε_{ALL3}	0.02 ± 0.29	−0.03 ± 0.31	0.04 ± 0.29	−0.03 ± 0.28	0.02 ± 0.25	−0.00 ± 0.25
R^2, p value	0.45, <0.001	0.32, 0.001–0.01	0.43, <0.001	0.33, 0.001–0.01	0.56, <0.001	0.47, <0.001

1980, the estimated trend of φ_{LMI} is highly sensitive to the sample size. For example, looking at the TCs in the IBTrACS best-track data during 1980–2013, the annual-mean φ_{LMI} (TC intensity is measured by maximum wind speed) in the western North Pacific shows a poleward migration trend (0.48 ± 0.46 latitude decade^{-1}), which is basically consistent with results of the previous studies (Kossin et al., 2014; Kossin et al., 2016). However, if the sample length is extended to 2020, the poleward migration trend decreases significantly (0.29 ± 0.38 latitude decade^{-1}) due to the low φ_{LMI} in 2014 and 2015 (Figure 1A; Table 1). Results based on other TC best-track data (i.e., JTWC, JMA, and CMA) also indicate that the poleward migration trend is no longer significant at the 95% confidence level when observations in 2014 and 2015 are considered (Table 1; Figures 1B–F) except

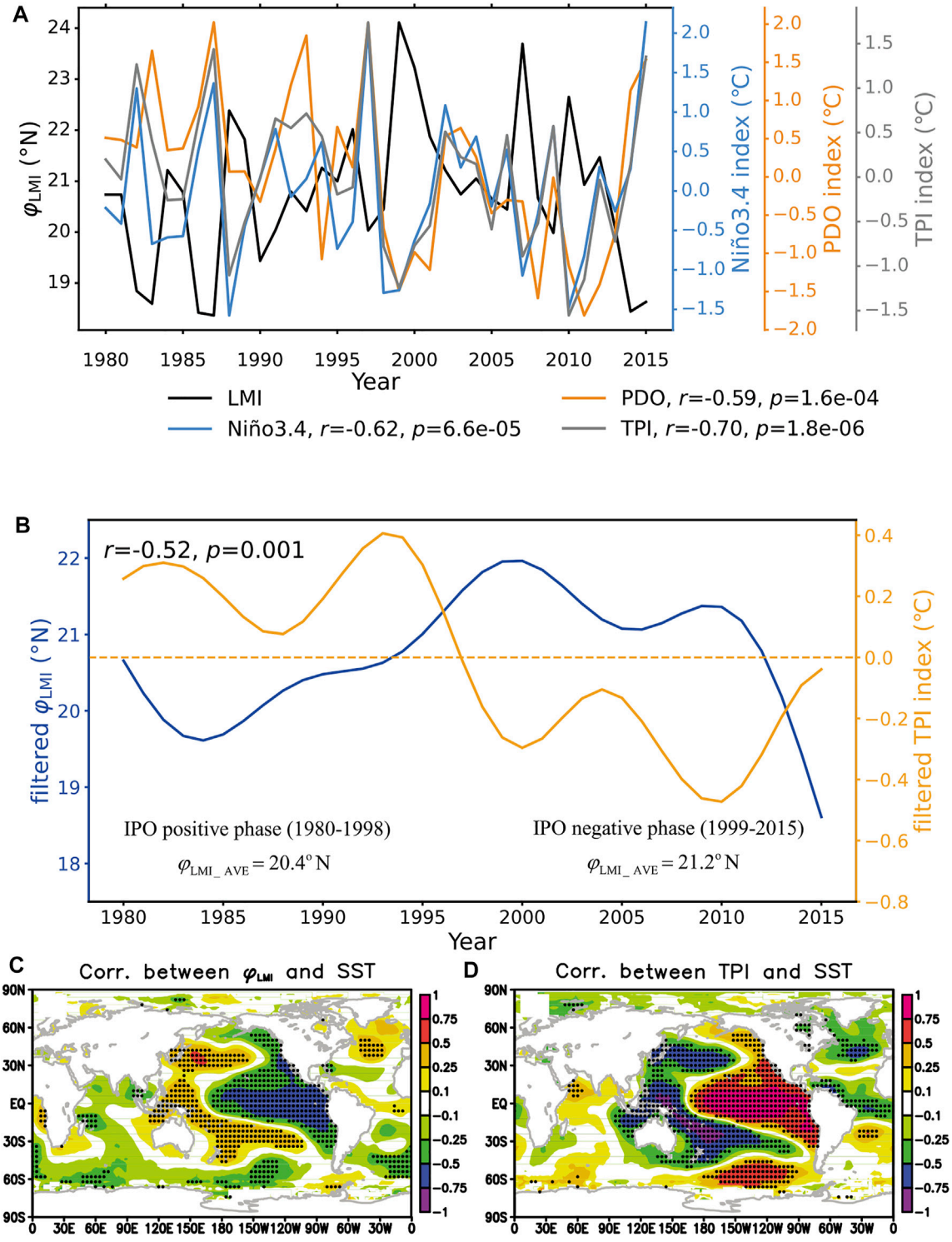

FIGURE 2
Relationship between the location of LMI over the WNP and the IPO. **(A)** Time series of annual-mean φ_{LMI} from the IBTrACS best-track data (black line) and JASON-mean TPI (grey line), Niño3.4 index (blue line), PDO (orange line); **(B)** Low pass filtered time series of TPI (orange line) and φ_{LMI} (blue line); **(C)** map of correlation coefficient between the annual-mean φ_{LMI} and JASON SST; and **(D)** map of correlation coefficient between the JASON TPI and JASON SST. The correlation coefficients (i.e., *r*) between φ_{LMI} and TPI or filtered TPI, and the *p*-value (i.e., *p*) for testing the hypothesis of no correlation are also shown in Figures 2A,B (annotated values). A 13-years Chebyshev low-pass filter is applied to obtain the filtered version of the two indices. The positive IPO phase corresponds to the period when the filtered TPI is no less than 0 °C (i.e., 1980–1998), while the IPO negative phase corresponds to the period when the filtered TPI is less than 0 °C (i.e., 1999–2015). The time-averaged φ_{LMI} in the two IPO phases are presented in Figure 2B (annotated values). Dotted areas in Figures 2C,D denote that the differences are significant at/above the 95% confidence level by the Student's *t* test.

HKO. More importantly, further analysis suggests that, rather than anthropogenic forcing, it is the natural variability that plays a critical role in modulating the migration of WNP TC track during the past 41 years.

3.2 Relationship between IPO and WNP TC migration

The variability of the WNP TC activity has received a large amount of attention during the past 2 decades, and many studies have linked TC track variability to ENSO (Camargo et al., 2007a; Liu & Chan, 2008) on interannual timescale. In recent years, the PDO has been found to have important influences on large-scale flow patterns and thus the TC track variability over the WNP (Liu & Chan, 2008; Mei et al., 2015). Here, averages of the ENSO (Niño-3.4), PDO, IPO (IPO tripole index, TPI) (Henley et al., 2015) indices are taken over July-November (JASON), which is considered as the peak TC season (about 80% of annual WNP TCs occur in these months) (Kossin et al., 2016). As expected, there is an inverse relationship between φ_{LMI} and the two indices (i.e., Niño-3.4 and PDO) with the correlation coefficients of −0.62 and −0.59 respectively, which indicate ENSO and PDO both have strong impacts on TC migration (Figure 2A). Moreover, compared with the ENSO and PDO, the IPO plays an even more important role in determining the WNP TC migration with a correlation coefficient of −0.70 between φ_{LMI} and TPI. Almost all the peaks of IPO negative (positive) values correspond to high (low) values of φ_{LMI} and φ_{LMI} increased dramatically during the transition of the IPO from positive to negative phase in the late 1990s (Meehl et al., 2013; Henley et al., 2015) (Figure 2A). Note that the low φ_{LMI} in 2014 and 2015 correspond to positive values of the TPI, which makes the poleward migration trend of φ_{LMI} insignificant when the study period is changed from 1980–2013 to 1980–2015. On the other hand, as the low frequency component of the IPO signal can be obtained by applying a 13-years Chebyshev low-pass filter to TPI (Henley et al., 2015), we calculated the filtered φ_{LMI} using the same filter, and found that the correlation coefficient between the filtered TPI and the filtered φ_{LMI} is −0.52, which is significant at the 99% confidence level (Figure 2B). This result strongly suggests that there is a significant inverse correlation between IPO and the WNP TC migration on interdecadal timescale. In addition, the map of correlation coefficient between φ_{LMI} and SST presents a pattern highly similar to the map of correlation coefficient between TPI and SST (Figures 2C,D). The latter displays a typical IPO pattern (see Figure 1 in the Henley et al., 2015) and thus provides robust evidence supporting the strong relationship between the WNP TC migration and IPO.

To further compare the contributions of various natural variabilities to the WNP TC migration, we calculate the residuals of annual-mean φ_{LMI} regressed onto the JASON-mean Niño-3.4, PDO, and TPI indices (i.e., $\varepsilon_{Niño\text{-}3.4}$, ε_{PDO}, and ε_{TPI}), respectively. The residuals of the trivariate regression of φ_{LMI} onto the three indices (i.e., ε_{ALL3}) are also calculated. For instance, ENSO is removed from the φ_{LMI} time series by regressing the φ_{LMI} series onto the Niño-3.4 index averaged over the peak TC season (July-November), and the residuals are analyzed. When the PDO and IPO variabilities are removed respectively, the residual TC migration rates (i.e., ε_{PDO}, and ε_{TPI}) are found to decrease substantially for various best-track data (Table 1; Figure 3). This suggests that the PDO and IPO considerably contribute to the TC migration rate. Moreover, as expected, the regression coefficients (i.e., R^2) are statistically significant, and the JASON-mean ENSO, PDO, IPO, and all these three indices together respectively explain 34.5%, 24.0%, 44.7%, and 44.7% of the φ_{LMI} variance in the IBTrACS best-track data (Table 1). These results further suggest that natural variability, especially IPO (Wang et al., 2013; Henley et al., 2015), whose contribution to the change of φ_{LMI} is similar to the total contribution of the three indices, is playing a critical role in the observed TC migration. Furthermore, when the IPO variability (i.e., time series of the TPI) is removed, the residual TC migration rate decreases significantly from 0.29 ± 0.38 latitude decade^{-1} (i.e., φ_{LMI} trend which is significant at 76% confidence level) to 0.03 ± 0.29 latitude decade^{-1} (see φ_{LMI} and ε_{TPI} in Table 1). This indicates that the poleward migration trend of the WNP TC track does not occur outside the IPO variability based on the observational records (1980–2020), and thus provides evidence against the proposed conclusions of previous studies on the contribution of anthropogenic factors to the TC poleward migration ((Kossin et al., 2014; Kossin et al., 2016). In this study, rather than studying the φ_{LMI} trend, we put emphasis on the close relationship between TC migration and IPO, especially the modulation of IPO on the WNP TC migration.

Despite the strong agreement between the two indices of PDO and IPO ($r = 0.75$), the IPO index (i.e., TPI) is based on the difference between SST averaged over the central equatorial Pacific and that over the northwestern and southwestern Pacific, and thus is substantially different from the PDO index which is mainly determined by SST in the North Pacific (north of 20oN) (Mantua et al., 1997). Thus, compared with the PDO index, the IPO index is more related to meridional and zonal gradients of SST over the WNP. The interdecadal changes of the SST gradients and related spatial SST distribution pattern make large contributions to the WNP TC migration, which will be discussed in detail in the next section.

3.3 Possible trend of WNP TC migration in future under global warming

As mentioned above, our observational results imply that the anthropogenic forcing does not contribute significantly to the observed WNP TC migration as expected. This also does not necessarily mean that the anthropogenic factors (e.g., global warming induced by greenhouse gases) will not significantly contribute to the poleward shift of the WNP TC in the future, since it is difficult to distinguish the contributions of anthropogenic

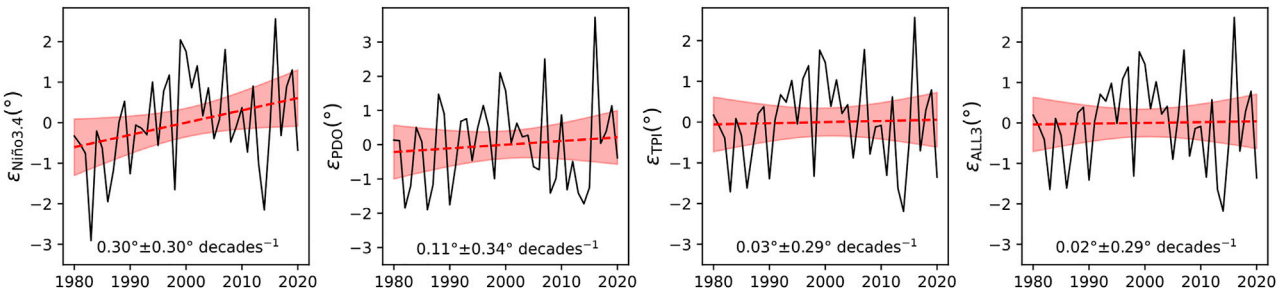

FIGURE 3
Possible effects of the three modes of variability on the migration of the latitude of LMI. Time series of **(A)** residuals of the single-variate of annual-mean φ_{LMI} onto JASON-mean Niño-3.4 index, **(B)** residuals of the single-variate of annual-mean φ_{LMI} onto JASON-mean PDO index, **(C)** residuals of the single-variate of annual-mean φ_{LMI} onto JASON-mean TPI index, and **(D)** residuals of the trivariate of annual-mean φ_{LMI} onto JASON-mean Niño-3.4, PDO, and TPI indices. Linear trend lines (dashed) are shown with their 95% two-sided confidence intervals (shaded), which are also shown by annotated values.

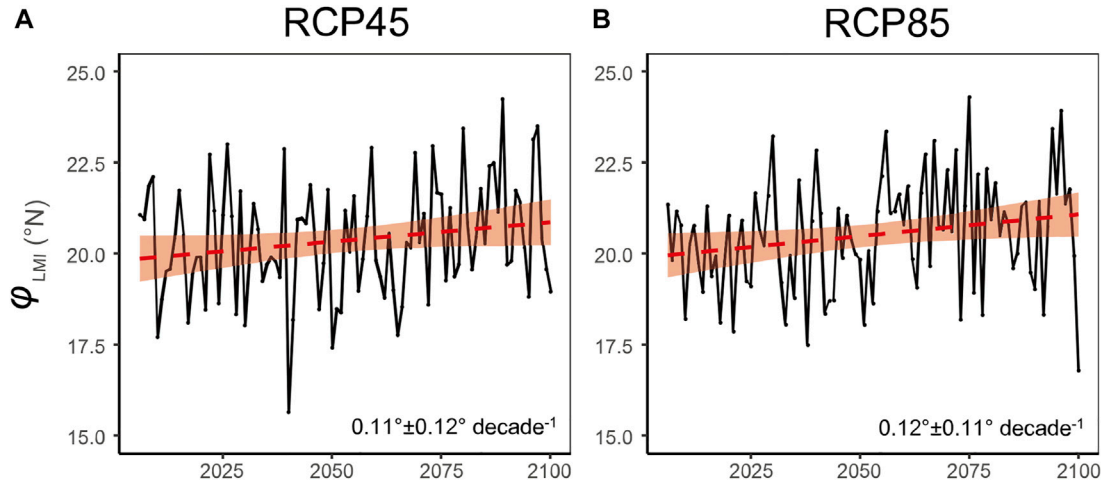

FIGURE 4
Projected migrations of the WNP TC in future under the two representative emission scenarios. Time series of annual-mean φ_{LMI} from WNP TCs explicitly generated in the 14 CMIP5 twenty-first-century **(A)** RCP4.5 and **(B)** RCP8.5 projection simulations.

forcing and natural variability based on the short time-period records (Allen et al., 2014; Lucas et al., 2014; Boo et al., 2015).

Thanks to the relatively long period (2006–2100) of RCP4.5 and RCP8.5 scenarios which is much longer than the period during which the known modes of natural variability are derived, it is relatively robust and reliable to draw the conclusions on the influence of anthropogenic forcing by using the results of these 14 CMIP5 models under the RCP4.5 and RCP8.5 scenarios. In the RCP4.5 projection simulations, the projected rate of migration of φ_{LMI} (0.11°±0.12° decade^{-1}) is insignificant just under the 95% confidence level (Figure 4). The difference in φ_{LMI} between RCP8.5 and RCP4.5 scenarios is hardly distinguishable, although the φ_{LMI} in RCP8.5 scenario (0.12°±0.11° decade^{-1}) is just at the 95% confidence level (Figure 4). Thereby, the projected rates of WNP TC migration are closely related to the carbon emission intensity, as the migration rates, in terms of φ_{LMI} trends, increase with the carbon emission intensity (Figure 4). In RCP4.5 scenario, the global warming remains unable to produce significant trend, indicating that the observed insignificant trend is confirmed in the model.

3.4 Possible mechanisms for the impact of IPO on WNP TC migration on interdecadal timescales

The φ_{LMI} of a TC is determined by TC genesis positon, TC intensity evolution and TC track pattern. The first determines the starting position of a TC during its lifetime, the second evolves before LMI is reached and controls when the LMI would occur during the TC lifetime, and the third determines the path of the

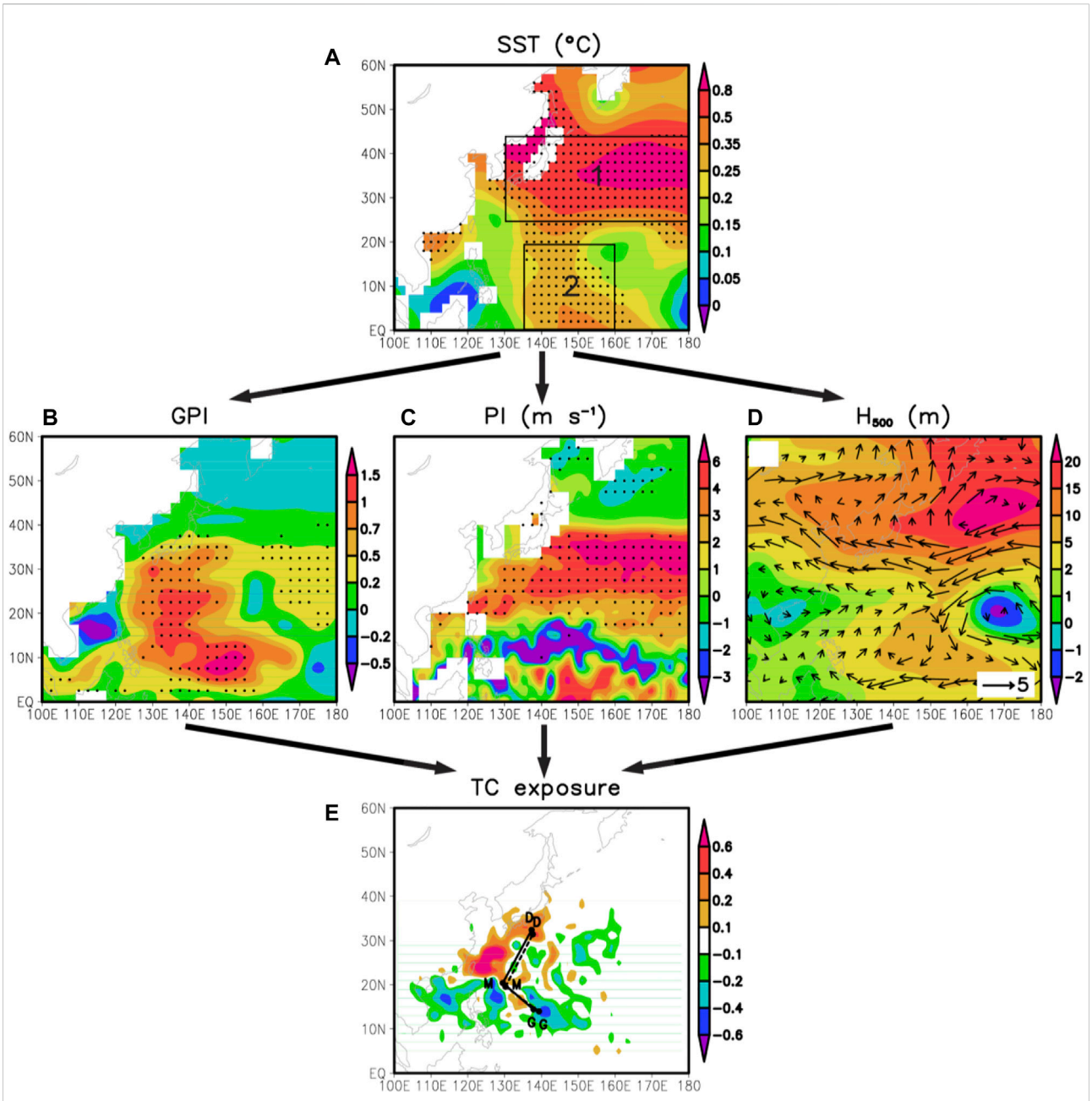

FIGURE 5
Differences in annual-mean JASON SST, GPI, PI, large-scale circulation, and TC exposure between negative IPO phase and positive IPO phase. **(A)** SST (°C), **(B)** GPI, **(C)** PI (m s^{-1}), **(D)** 500-hPa geopotential height (shaded; m) and 850–300 hPa vertical-mean wind (vectors; m s^{-1}), and **(E)** TC exposure (number of days of exposure per year per 2°×2° latitude–longitude grid box) and the positions of TC genesis (G), lifetime maximum intensity (M), and disappearance (D), which are depicted in dotted line in the positive IPO phase and in solid line in the negative IPO phase. The IPO negative phase refers to the period of 1980-1998, and the IPO positive phase refers to the period of 1999–2015. Dotted areas denote that the differences are significant at/above the 99% confidence level by the Student's *t* test. Black boxes indicate the two main regions where SST differences are significant at/above the 99% confidence (Region 1: 25°N-45°N, 130°E-180°E; Region 2: 0°N-20°N, 135°E-160°E).

TC and thus controls where the LMI would possibly occur during the TC lifetime. In this study, these three factors can be analyzed from the aspects of GPI, PI, and large-scale environmental flow respectively (Sun et al., 2020). Firstly, the GPI is widely used to analyze spatial distribution of TC genesis potential and the influence of environmental factors on tropical cyclogenesis (Camargo et al., 2007b). Secondly, PI is a known major factor modulating the TC intensity evolution (Emanuel, 1999). Thirdly,

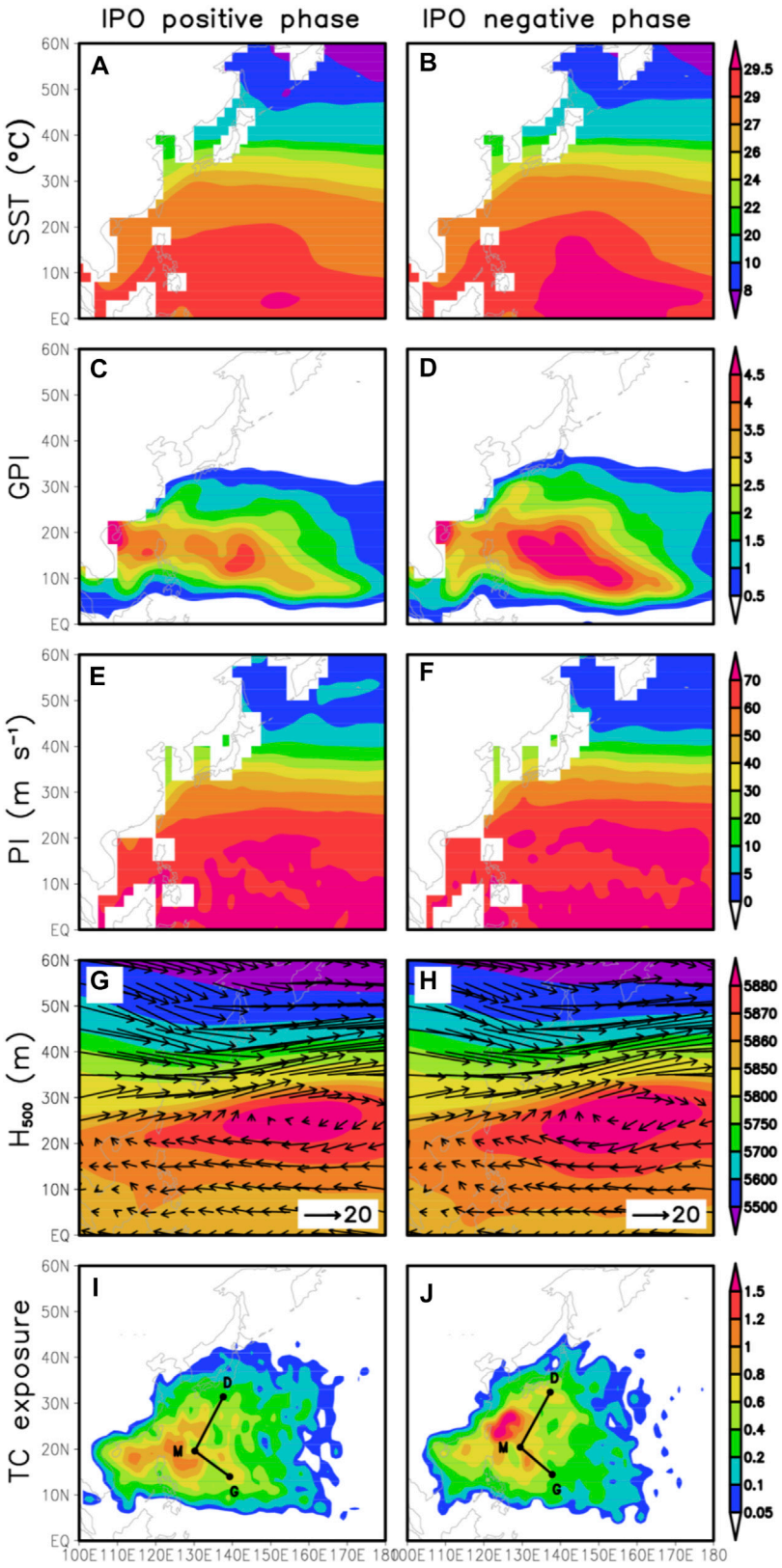

FIGURE 6
Annual-mean JASON SST, GPI, PI, large-scale circulation, and TC exposure during the positive IPO phase **(A,C,E and G)** and negative IPO phase **(B,D,F and H)**. **(A,B)** SST (°C); **(C,D)** GPI; **(E,F)** PI (m s^{-1}); **(G,H)** 500-hPa geopotential height (shaded; m) and 850–300 hPa vertically averaged wind (vectors; m s^{-1}); and **(I,J)** TC exposure (number of days of exposure per year per 2°×2° latitude–longitude grid box) and the positions of TC genesis (G), lifetime maximum intensity (M), and disappearance (D).

WNP TCs are usually steered by large-scale environmental flow, especially the flow in the main TC activity region (Chan & Gray, 1982; Sun et al., 2015), which modulates the geographical properties of TC track over the WNP. Therefore, the change of φ_{LMI} can always be attributed to changes in the GPI, PI and large-scale environmental flow.

Consistent with the previous studies (Burgman et al., 2008; Chen et al., 2008; Lee & McPhaden, 2008; Meehl & Arblaster, 2012; Henley et al., 2015), the IPO transferred from positive to negative phase in the late 1990s after the 1997–98 El Niño event. Thus, the period of 1980–1998 (1999–2015) can be considered as the positive (negative) IPO phase on interdecadal timescale (Figure 2B). Moreover, the time-averaged φ_{LMI} in the negative IPO phase (21.2°N) is notably higher than that in the positive IPO phase (20.4°N), which is significant above the 95% confidence level by the Two-sample *t*-test. The positive and negative phases of IPO are characterized by different regional patterns (Power et al., 1999; Folland et al., 2002; Henley et al., 2015), which are expected to play an important role in determining the GPI and PI spatial distributions and the large-scale environmental flow in the main TC activity region, and eventually affect φ_{LMI} of TCs over the WNP. However, based on what we understand, little is known about the impact of the regional pattern of IPO on the TC track migration. To further investigate the linkage between IPO and the WNP TC migration, we compare SST, GPI, PI, large-scale circulation, and TC exposure during the negative and positive IPO phases (Figure 5 and Figure 6). Note that, TC exposure is defined as the number of days per year per 2×2 latitude–longitude grid box when a TC center is located in that grid box.

During the transitional period from the positive IPO phase to negative IPO phase over the WNP, there are two main regions (Region 1 25°N-45°N, 130°E-180°E; Region 2 0°N-20°N, 135°E-155°E) where positive SST anomalies are significant at/above the 99% confidence level (Figure 5A). At first, the higher SST in Region 1 and Region 2 contribute to the significant increase of GPI in the three ocean areas (i.e., an ocean area to the south of Japan, an ocean area near the equator, and an ocean area near the central North Pacific). Compared with the first area that is to the north of the main WNP TC genesis area (see Figures 6C,D), the latter two areas are relatively farther from the main genesis region of WNP TC and thus contribute relatively smaller to the migration of TC genesis position (Figure 5B). Under the joint effects of GPI changes in the three areas, the time-averaged TC genesis position shifts poleward by 0.47 latitude (Figure 5E). Moreover, the higher SST in Region 1 leads to a relatively higher PI that favors further development of TCs at the high latitudes over the region (Figure 5C and Figures 6E,F), and eventually leads to the poleward shift of φ_{LMI}. More importantly, the higher SST in Region 2 induces positive geopotential height anomalies in this region as the ocean warming is favorable for the development of the deep warm high (i.e., WPSH) in the non-equatorial region (>5°N), which favors westward expansion of the WPSH over *Region 2* (Figure 5D and Figures 6G,H). The anticyclonic anomaly in the western boundary of the westward-expanded WPSH contributes to increases in the northward steering flow over the area of 10°N-22°N, 120°E-135°E, which tends to promote northward turning of westward moving TCs over the area (Figure 5D). In addition to the poleward shift of φ_{LMI}, the intensified northward steering flow also contributes to the increase in TC exposure over the regions of Taiwan, Ryukyu Islands, the southern coast of Japan, and the southeastern coast of China, but decreases TC exposure in the regions of Hainan, Vietnam, and Philippines (Figure 5E). Note that the response of equatorial circulations to higher SST is substantially different to that of mid- and low-latitude circulations. Over the equatorial area in Region 2, the prevailing easterly winds basically agree with the theory of Gill model (Gill, 2010), which indicates that an equatorial heating (e.g., SST warming) produces easterly flow over the eastern region of the heating (Figure 5D). Overall, due to the response of GPI, PI and large-scale flow to IPO, the WNP TCs tend to originate and intensify at high latitudes and turn poleward over certain regions, which contributes to the poleward shift of the location of LMI during the IPO transition period from positive to negative phase in the late 1990s.

4 Conclusion

This paper investigates that IPO impact on Migration of Tropical Cyclone Track over the Western North Pacific. We found that the location where TCs reach their lifetime maximum intensity (LMI) moved northward with a trend of 0.29 ± 0.38 latitude decade-1 from 1980 to 2020. But the trend was not significant, which is consistent across different datasets. The correlation analysis shows that the correlation coefficient between TC latitude at the time of LMI (φ_{LMI}) and JASON-mean TPI from 1980 to 2020 is as high as −0.70, and the PDO is −0.59, and the Niño3.4 index is −0.62. When applying a 13-years Chebyshev low-pass filter to TPI and φ_{LMI}, the correlation coefficient is −0.52, passed the 95% significance test. In order to study the effect of these natural variability on the motion of φ_{LMI}, we remove these three natural variability trends from φ_{LMI}. and the JASON-mean ENSO, PDO, IPO, and all these three indices together respectively explain 34.5%, 24.0%, 44.7%, and 44.7% of the φ_{LMI} variance. When the IPO variability is removed, the residual TC migration rate decreases significantly from 0.29 ± 0.38 latitude decade-1 to 0.03 ± 0.29 latitude decade-1. This phenomenon is inconsistent with the previous conclusion that human factors contribute to the polar movement of TC. Therefore, 14 CMIP5 models under the RCP4.5 and RCP8.5 Scenarios were used to investigate the anthropogenic contribution of TC to polar mobility. The results show that the poleward movement trend of TC is not as obvious as that during the observation period. In order to further explore why IPO affects TC poleward movement, genesis potential index (GPI),

potential intensity (PI), and large-scale environmental flow are analyzed respectively because of their contribution to TC genesis position, TC intensity evolution and TC track pattern. There are two main regions (Region 1 25°N-45°N, 130°E-180°E; Region 2 0°N-20°N, 135°E-155°E) where positive SST anomalies are significant at above the 99% confidence level, which contribute to the significant increase of GPI in the three ocean areas and induce a relatively higher PI that promotes further extension of TCs at the high latitudes over the region. The higher SST in Region 2 contributes to positive geopotential height anomalies that can lead to increases in the northward steering flow over the area of 10°N-22°N, 120°E-135°E, which helps TC's poleward shift.

In the following work, we will continue to study the contribution of various natural variability, including IPO, to the poleward movement of TC in future scenarios. We will also continue to use the latest numerical weather patterns on the impact of human activities on the TC for further explanation. We believe that human activity to a certain extent, also affect the change of the TC. However, further research is needed to determine whether this effect will affect TC as human activities affect natural variability, or directly affect TC itself.

Data availability statement

The original contributions presented in the study are included in the article/Supplementary Material, further inquiries can be directed to the corresponding author.

Author contributions

YS conceived the project. SL analyzed the results, produced the figures, and wrote the manuscript with contributions from ZZ, YUS and YIS wrote the codes on produced the TC data in CMIP5 models. ZZ advised on physical interpretation of IPO Modulation on TC track Migration.

Funding

This work is supported by the National Natural Science Foundation of China (No. 42075035 and 42075011).

Conflict of interest

The authors declare that the research was conducted in the absence of any commercial or financial relationships that could be construed as a potential conflict of interest.

Publisher's note

References

Allen, R. J. Norris, J. R. and Kovilakam, M. (2014). Influence of anthropogenic aerosols and the Pacific decadal oscillation on tropical belt width. *Nat. Geosci.* 7, 270–274. doi:10.1038/ngeo2091

Boo, K.-O. Booth, B. B. Byun, Y.-H. Lee, J. Cho, C. Shim, S., et al. (2015). Influence of aerosols in multidecadal SST variability simulations over the North Pacific. *J. Geophys. Res. Atmos.* 120, 517–531. doi:10.1002/2014jd021933

Burgman, R. J. Clement, A. C. Mitas, C. M. Chen, J. and Esslinger, K. (2008). Evidence for atmospheric variability over the Pacific on decadal timescales. *Geophys. Res. Lett.* 35, L01704. doi:10.1029/2007GL031830

Camargo, S. J. (2013). Global and regional aspects of tropical cyclone activity in the CMIP5 models. *J. Clim.* 26, 9880–9902. doi:10.1175/jcli-d-12-00549.1

Camargo, S. J. Kmanuel, K. A. and Sobel, A. H. (2007b). Use of a genesis index to diagnose ENSO effects on tropical cyclone genesis. *J. Clim.* 20, 4819–4834. doi:10.1175/JCLI4282.1

Camargo, S. J. Robertson, A. W. Gaffney, S. J. Smyth, P. and Ghil, M. (2007a). Cluster analysis of typhoon tracks. Part II: Large-scale circulation and ENSO. *J. Clim.* 20, 3654–3676. doi:10.1175/jcli4203.1

Cardon, O. D. Maarten, V. A. Joern, B. Maureen, F. Glenn, M. and Mechler, R. (2012). "Determinants of risk: Exposure and vulnerability." in *Managing the risks of extreme events and disasters to advance climate change adaptation*. Cambridge, United Kingdom: Cambridge University Press.

Chan, J. C. L. and Gray, W. M. (1982). Tropical cyclone movement and surrounding flow relationships. *Mon. Wea. Rev.* 110, 1354–1374. doi:10.1175/1520-0493(1982)110<1354:tcmasf>2.0.co;2

Chen, J. Del Genio, A. D. Carlson, B. E. and Bosilovich, M. G. (2008). The spatiotemporal structure of twentieth-century climate variations in observations and reanalyses. Part II: Pacific pan-decadal variability. *J. Clim.* 21, 2634–2650. doi:10.1175/2007jcli2012.1

Christensen, J. H. (2013). "Climate phenomena and their relevance for future regional climate change." in *Climate change 2013: The physical science basis. Contribution of working group I to the fifth assessment report of the intergovernmental panel on climate change*. Cambridge: Cambridge University Press.

Dee, D. P. Uppala, S. M. Simmons, A. J. Berrisford, P. Poli, P. Kobayashi, S., et al. (2011). The ERA-interim reanalysis: Configuration and performance of the data assimilation system. *Q. J. R. Meteorol. Soc.* 137, 553–597. doi:10.1002/qj.828

Emanuel, K. A. (1999). Thermodynamic control of hurricane intensity. *Nature* 401, 665–669. doi:10.1038/44326

Folland, C. K. Renwick, J. A. Salinger, M. J. and Mullan, A. B. (2002). Relative influences of the interdecadal pacific oscillation and ENSO on the south pacific convergence zone. *Geophys. Res. Lett.* 29, 21-1–21-4. doi:10.1029/2001gl014201

Gill, A. E. (2010). Some simple solutions for heat-induced tropical circulation. *Q. J. R. Meteorol. Soc.* 106, 447–462. doi:10.1002/qj.49710644905

Henley, B. J. Gergis, J. Karoly, D. J. Power, S. Kennedy, J. and Folland, C. K. (2015). A tripole index for the interdecadal pacific oscillation. *Clim. Dyn.* 45, 3077–3090. doi:10.1007/s00382-015-2525-1

Ho, C.-H. Baik, J.-J. Kim, J.-H. Gong, D.-Y. and Sui, C. H. (2004). Interdecadal changes in summertime typhoon tracks. *J. Clim.* 17, 1767–1776. doi:10.1175/1520-0442(2004)017<1767:icistt>2.0.co;2

Kalnay, E. Kanamitsu, M. Kistler, R. Collins, W. Deaven, D. Gandin, L., et al. (1996). The NCEP/NCAR 40-year reanalysis project. *Bull. Am. Meteorol. Soc.* 77, 437–471. doi:10.1175/1520-0477(1996)077<0437:tnyrp>2.0.co;2

Knapp, K. P. Kruk, M. C. Levinson, D. H. Diamond, H. J. and Neumann, C. J. (2010). The international best track archive for climate stewardship (IBTrACS): Unifying tropical cyclone data. *Bull. Am. Meteorol. Soc.* 91, 363–376. doi:10.1175/2009bams2755.1

Knapp, K. R. Diamond, H. J. Kossin, J. P. Kruk, M. C. and Schreck, C. J. (2018). International best track archive for climate stewardship (IBTrACS) project, version 4. *NOAA Natl. Centers Environ. Inf.* doi:10.25921/82ty-9e16

Knapp, K. R. and Kruk, M. C. (2010). Quantifying interagency differences in tropical cyclone best track wind speed estimates. *Mon. Weather Rev.* 138, 1459–1473. doi:10.1175/2009mwr3123.1

Knutson, T. R. McBride, J. L. Chan, J. Emanuel, K. Holland, G. Landsea, C., et al. (2010). Tropical cyclones and climate change. *Nat. Geosci.* 3, 157–163. doi:10.1038/ngeo779

Kossin, J. P. Camargo, S. J. and Sitkowski, M. (2010). Climate modulation of North Atlantic hurricane tracks. *J. Clim.* 23, 3057–3076. doi:10.1175/2010jcli3497.1

Kossin, J. P. Emanuel, K. A. and Camargo, S. J. (2016). Past and projected changes in western North Pacific tropical cyclone exposure. *J. Clim.* 29, 5725–5739. doi:10.1175/jcli-d-16-0076.1

Kossin, J. P. Emanuel, K. A. and Vecchi, G. A. (2014). The poleward migration of the location of tropical cyclone maximum intensity. *Nature* 509, 349–352. doi:10.1038/nature13278

Lee, T.-C. Knutson, T. R. Kamahori, H. and Ying, M. (2012). Impact of climate change on tropical cyclones in the Western North pacific basin. Part I: Past observations. *Trop. Cyclone Res. Rev.* 1, 213–230. doi:10.6057/2012TCRR02.09

Lee, T.-C. Knutson, T. R. Nakaegawa, T. Ying, M. and Cha, E. J. (2020). Third assessment on impacts of climate change on tropical cyclones in the Typhoon Committee Region – Part I: Observed changes, detection and attribution. *Trop. Cyclone Res. Rev.* 9, 1–22. doi:10.1016/j.tcrr.2020.03.001

Lee, T. and McPhaden, M. J. (2008). Decadal phase change in largescale sea level and winds in the Indo-Pacific region at the end of the 20th century. *Geophys. Res. Lett.* 35, L01605. doi:10.1029/2007GL032419

Liu, K. S. and Chan, J. C. L. (2013). Inactive period of western North Pacific tropical cyclone activity in 1998–2011. *J. Clim.* 26, 2614–2630. doi:10.1175/jcli-d-12-00053.1

Liu, K. S. and Chan, J. C. L. (2008). Interdecadal variability of western North Pacific tropical cyclone tracks. *J. Clim.* 21, 4464–4476. doi:10.1175/2008jcli2207.1

Lucas, C. Timbal, B. and Nguyen, H. (2014). The expanding tropics: A critical assessment of the observational and modeling studies. *WIREs Clim. Change* 5, 89–112. doi:10.1002/wcc.251

Mantua, N. J. Hare, S. R. Zhang, Y. Wallace, J. M. and Francis, R. C. (1997). A Pacific interdecadal climate oscillation with impacts on salmon production. *Bull. Amer. Meteor. Soc.* 78, 1069–1079. doi:10.1175/1520-0477(1997)078<1069:apicow>2.0.co;2

Meehl, G. A. and Arblaster, J. M. (2012). Relating the strength of the tropospheric biennial oscillation (TBO) to the phase of the Interdecadal Pacific Oscillation (IPO). *Geophys. Res. Lett.* 39, L20716. doi:10.1029/2012GL053386

Meehl, G. A. Hu, A. Arblaster, M. J. Fasullo, J. and Trenberth, K. E. (2013). Externally forced and internally generated decadal climate variability associated with the interdecadal pacific oscillation. *J. Clim.* 26, 7298–7310. doi:10.1175/jcli-d-12-00548.1

Mei, W. Xie, S.-P. Zhao, M. and Wang, Y. (2015). Forced and internal variability of tropical cyclone track density in the western North Pacific. *J. Clim.* 28, 143–167. doi:10.1175/JCLI-D-14-00164.1

Peduzzi, P. Chatenoux, B. Dao, H. De Bono, A. Herold, C. Kossin, J., et al. (2012). Tropical cyclones: Global trends in human exposure, vulnerability and risk. *Nat. Clim. Change* 2, 289–294. doi:10.1038/nclimate1410

Power, S. Casey, T. Folland, C. Colman, A. and Mehta, V. (1999). Inter-decadal modulation of the impact of ENSO on Australia. *Clim. Dyn.* 15, 319–324. doi:10.1007/s003820050284

Shen, Y. Sun, Y. Zhong, Z. Liu, K. and Shi, J. (2018). Sensitivity experiments on the poleward shift of tropical cyclones over the western North pacific under warming ocean conditions. *J. Meteorol. Res.* 32, 560–570. doi:10.1007/s13351-018-8047-0

Smith, T. M. and Reynolds, R. W. (2003). Extended reconstruction of global sea surface temperatures based on COADS data (1854–1997). *J. Clim.* 16, 1495–1510. doi:10.1175/1520-0442-16.10.1495

Sun, Y. Zhong, Z. Li, T. Yi, L. Shi, J. Shen, Y., et al. (2020). Superiority of mega ENSO index in the seasonal prediction of tropical cyclone activity over the western North pacific. *Earth Space Sci.* 7, e2019EA001009. doi:10.1029/2019ea001009

Sun, Y. Zhong, Z. Yi, L. Li, T. Chen, M. Wan, H., et al. (2015). Dependence of the relationship between the tropical cyclone track and western pacific subtropical high intensity on initial storm size: A numerical investigation. *J. Geophys. Res. Atmos.* 120, 11451–11467. doi:10.1002/2015jd023716

Wang, B. Liu, J. Kim, H. J. Webster, P. J. Yim, S. Y. and Xiang, B. (2013). Northern Hemisphere summer monsoon intensified by mega-El Niño/southern oscillation and Atlantic multidecadal oscillation. *Proc. Natl. Acad. Sci. U. S. A.* 110, 5347–5352. doi:10.1073/pnas.1219405110

Wang, C. and Wang, X. (2013). Classifying El Niño Modoki I and II by different impacts on rainfall in southern China and typhoon tracks. *J. Clim.* 26, 1322–1338. doi:10.1175/jcli-d-12-00107.1

Wang, R. Wu, L. and Wang, C. (2011). Typhoon track changes associated with global warming. *J. Clim.* 24, 3748–3752. doi:10.1175/jcli-d-11-00074.1

Zhang, W. Graf, H.-F. Leung, Y. and Herzog, M. (2012). Different El Niño types and tropical cyclone landfall in east asia. *J. Clim.* 25, 6510–6523. doi:10.1175/jcli-d-11-00488.1